

# Tin Tungstate Nanoparticles: A Photosensitizer for Photodynamic Tumor Therapy

Carmen Seidl<sup>†</sup>, Jan Ungelenk<sup>‡</sup>, Eva Zittel<sup>†</sup>, Thomas Bergfeldt<sup>§</sup>, Jonathan P. Sleeman<sup>⊥</sup>, Ute Schepers<sup>†\*</sup>,  
and Claus Feldmann<sup>‡\*</sup>

<sup>†</sup>Institute of Toxicology and Genetics, Karlsruhe Institute of Technology (KIT), Hermann-von-Helmholtz-Platz 1, 76344 Eggenstein-Leopoldshafen (Germany), E-mail: [ute.schepers@kit.edu](mailto:ute.schepers@kit.edu)

<sup>‡</sup>Institute of Inorganic Chemistry, Karlsruhe Institute of Technology (KIT), Engesserstr. 15, 76131 Karlsruhe (Germany), E-mail: [claus.feldmann@kit.edu](mailto:claus.feldmann@kit.edu)

<sup>§</sup>Institute of Applied Materials Physics, Karlsruhe Institute of Technology (KIT), Hermann-von-Helmholtz-Platz 1, 76344 Eggenstein-Leopoldshafen (Germany)

<sup>⊥</sup>Medical Faculty Mannheim of the University of Heidelberg, Centre for Biomedicine and Medical Technology Mannheim (CBTM), Ludolf-Krehl-Str. 13-17, 68167 Mannheim (Germany)

## **– SUPPORTING INFORMATION –**

### **Content**

1. Analytical tools
  2. Synthesis of protamine-functionalized  $\beta$ -SnWO<sub>4</sub> nanoparticles
  3. *In vivo* tests of  $\beta$ -SnWO<sub>4</sub> nanoparticles with orthotopic breast cancer BALB/c mouse model
  4. Blood parameters
  5. Haematoxylin- and eosine-staining (progressive)
- References

## 1. Analytical tools

*Scanning electron microscopy (SEM)* was carried out with a Zeiss Supra 40 VP microscope. Diluted aqueous suspensions of as-prepared  $\beta$ -SnWO<sub>4</sub> were deposited on silicon wafers and evaporated. The acceleration voltage was in the range of 5–10 kV and the working distance was 3 mm.

*Transmission electron microscopy (TEM)*: Transmission electron microscopy (TEM) was conducted with a Philips CM200-FEG microscope operating at 200 kV. TEM samples were prepared by evaporating suspensions in ethanol on amorphous carbon (Lacey-)film suspended on copper grids. The deposition of the samples on the carbon (Lacey-)film copper grids was performed under Argon atmosphere in a glove-box.

*Dynamic light scattering (DLS)* was conducted with polystyrene cuvettes applying a Nanosizer ZS from Malvern Instruments.

*Zeta-potential measurements* were performed in polystyrene cuvettes applying a Nanosizer ZS from Malvern Instruments. To this purpose, aqueous suspensions were titrated from neutral to alkaline and acidic pH by addition of NaOH and HCl, respectively.

A *blue-LED light source* (LED lenser) was purchased by Zweibrüder Optoelectronics. The blue-light LED exhibited a total length of 66 mm, a diameter of 14 mm and a total weight of 19 g. It operated with a luminous flux of 12 lm and an irradiance of 0.2 W/cm<sup>2</sup> at a wavelength range of 440–500 nm and with  $\lambda_{max} = 465$  nm (*cf. main text: Figure 2a*).

*Diffuse reflectance spectra (UV-VIS)* of powders were recorded in a wavelength interval of 250–800 nm with a Varian Cary 100 spectrometer, equipped with an integrating sphere against BaSO<sub>4</sub> as a reference.

*Fourier-transform infrared spectroscopy (FT-IR)* was performed on a Bruker Vertex 70 FT-IR spectrometer using KBr pellets.

*Differential thermal analysis and thermogravimetry (DTA/TG)* were performed with a Netzsch STA 449 F3 applying  $\alpha$ -Al<sub>2</sub>O<sub>3</sub> as crucible material and reference sample. The samples were heated under N<sub>2</sub> flow to 800 °C with a heating rate of 1 K minute<sup>-1</sup>.

## 2. Synthesis of protamine-functionalized $\beta$ -SnWO<sub>4</sub> nanoparticles

Details regarding the synthesis were already reported elsewhere.<sup>1</sup> According to a typical recipe, SnCl<sub>2</sub> (417.1 mg, 2.2 mmol) was dissolved in 2.5 mL of carbonated water. Under vigorous magnetic stirring, this solution was added to 2.5 mL of an equimolar aqueous solution of Na<sub>2</sub>WO<sub>4</sub>·2H<sub>2</sub>O (725.7 mg) at ambient temperature. A bright yellow nanomaterial was generated immediately and the resulting suspension can be directly diluted with 20 mL of phosphate-buffered saline (PBS: 8.0 g/L NaCl; 0.2 g/L KCl; 1.42 g/L Na<sub>2</sub>HPO<sub>4</sub>; 1.78 g/L Na<sub>2</sub>HPO<sub>4</sub>·2H<sub>2</sub>O; 0.27 g/L KH<sub>2</sub>PO<sub>4</sub>) (*Figure S1*). The obtained nanomaterial was collected by centrifugation (15 min, 25,000 rpm), redispersed two times in PBS and centrifuged again for washing. Finally, the washed suspension was centrifuged for 2 minutes at 10,000 rpm in order to remove agglomerates. The obtained centrifugate represents an aqueous suspension of  $\beta$ -SnWO<sub>4</sub> nanoparticles showing diameters well below 20 nm and a mean diameter of 8( $\pm$ 2) nm (0.13 wt-%, 45% yield of dry powder) being fairly stable without any additional stabilizing agents (*cf. main text: Figure 1*).

To improve membrane penetration and cell uptake, the as-prepared  $\beta$ -SnWO<sub>4</sub> nanoparticles were coated with protamine.<sup>2</sup> To this concern, protamine solution (protamine sulfate from herring) was added drop-by-drop to the above described PBS suspension of the  $\beta$ -SnWO<sub>4</sub> nanoparticles in order to electrostatically bind the protamine to the particle surface (*Figure S1*). As a cationic biopolymer protamine adheres easily on the negatively charged  $\beta$ -SnWO<sub>4</sub> surface and naturally reduces the sum zeta potential to about -20 mV (*cf. main text: Figure 1c*). Note that only biocompatible solvents were used throughout the nanoparticle synthesis with PBS having the same pH (pH = 7.4) and the same osmotic pressure than human blood.

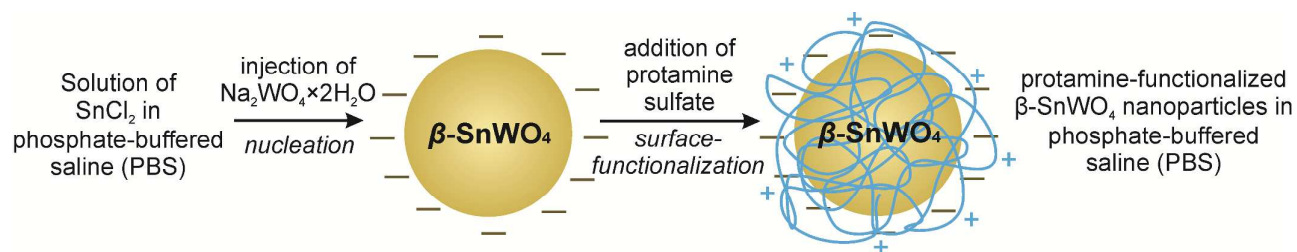


**Figure S1. Scheme illustrating the water-based synthesis of  $\beta$ -SnWO<sub>4</sub> nanoparticles as well as the subsequent protamine functionalization.**

The presence of protamine as a surface capping on the particle surface was validated by FT-IR spectra (*Figure S2*). While comparing to pure protamine as a reference, all characteristic vibrations ( $\nu$ (O-H): 3600-3000;  $\nu$ (C-H): 2950-2800;  $\nu$ (C=O): 1700-1500; fingerprint area: 1500-500) can be identified for the protamine-functionalized  $\beta$ -SnWO<sub>4</sub> nanoparticles as well. Thermogravimetry indicated the amount of protamine on the  $\beta$ -SnWO<sub>4</sub> nanoparticles (*Figure S3*). Accordingly, a first weight loss (6%) between

room temperature and 120 °C can be ascribed to an evaporation of water adhered on the particle surface. As a next step, a loss of about 34% by mass in a temperature range of 220–500 °C is related to the thermal decomposition of protamine. In view of the particle size ( $8\pm 2$  nm) of the as-prepared  $\beta$ -SnWO<sub>4</sub> nanoparticles, such a load of 30–35% is very typical for a protamine-type surface-capping. Non-capped as-prepared  $\beta$ -SnWO<sub>4</sub> nanoparticles as a reference show a similar evaporation of water, but no weight loss in the temperature range of 220–500 °C. The slight increase (about 4%) of mass at 300–350 °C is due to the oxidation of Sn<sup>2+</sup> to Sn<sup>4+</sup> in air according to the following reaction:  $\text{SnWO}_4 + \frac{1}{2}\text{O}_2 \rightarrow \text{SnO}_2 + \text{WO}_3$  (calculated: +4.4%).

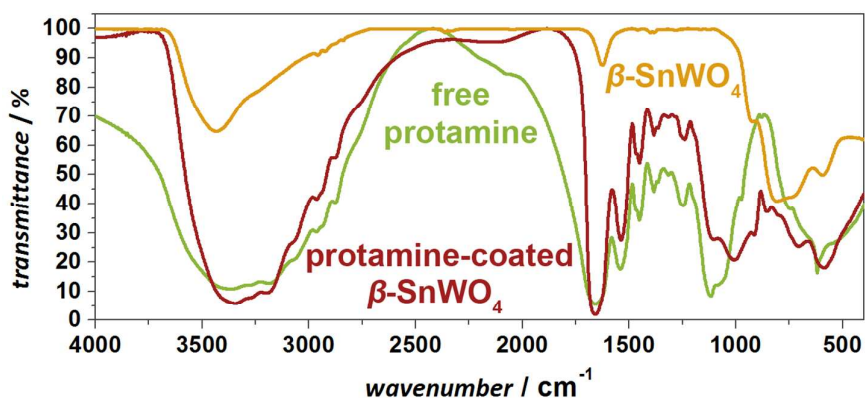


Figure S2. FT-IR spectrum of the protamine-functionalized  $\beta$ -SnWO<sub>4</sub> nanoparticles (as-prepared  $\beta$ -SnWO<sub>4</sub> nanoparticles and pure protamine as a reference).

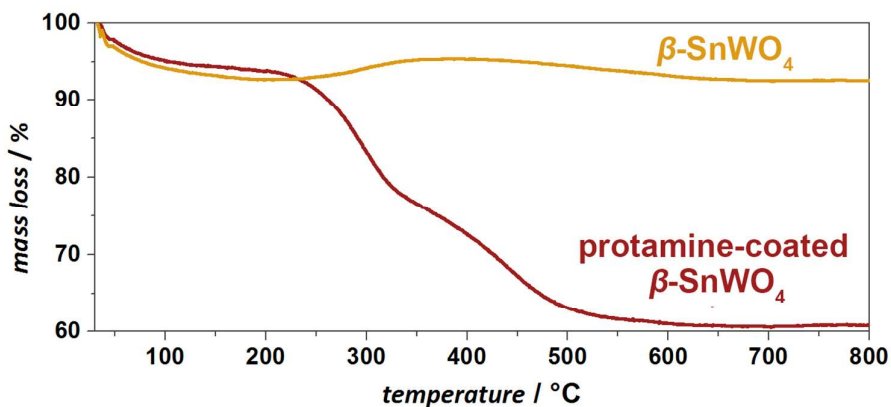


Figure S3. Thermogravimetry of the protamine-functionalized  $\beta$ -SnWO<sub>4</sub> nanoparticles (as-prepared  $\beta$ -SnWO<sub>4</sub> nanoparticles as a reference).

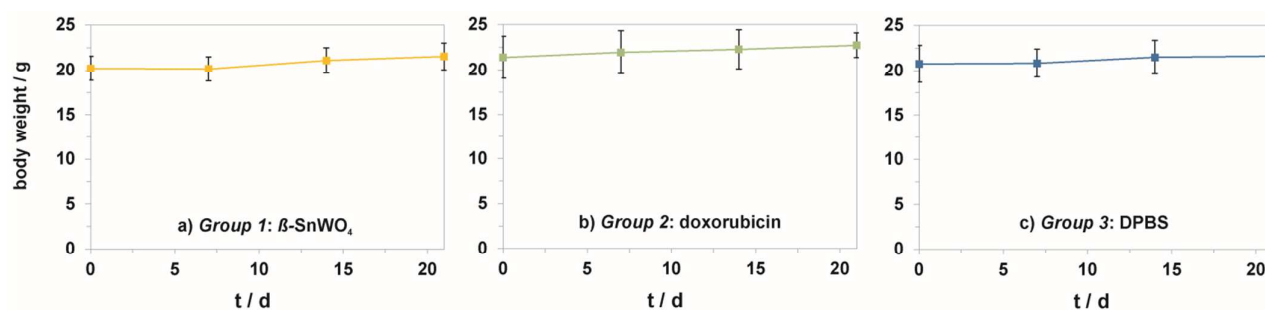
### 3. *In vivo* tests of $\beta$ -SnWO<sub>4</sub> nanoparticles with orthotopic breast cancer BALB/c mouse model

4T1 cells were maintained in DMEM medium supplemented with 10% FCS and 1% penicillin/streptomycin at 37 °C in a humidified incubator with 5% CO<sub>2</sub>.  $1 \cdot 10^6$  cells in 100  $\mu$ l of PBS were in-

jected orthotopically into the mammary fat pad of 8–12 weeks old female BALB/c mice. Before injection, cells were tested for mycoplasma with the VenorGeM<sup>®</sup> Mycoplasma Detection Kit. 11 days after tumor induction, mice were randomized into three experimental groups (six mice per group). Mice of *group 1* were treated intraperitoneally with protamine-functionalized  $\beta$ -SnWO<sub>4</sub> nanoparticles (23 mg/kg of body weight) trice a week for a total of seven doses. Subsequently, the tumor of mice from *group 1* was illuminated locally with a blue-LED point-light source ( $\lambda_{max} = 465$  nm) for 5 minutes. Control groups were treated with PBS (*group 3*) or doxorubicin (*group 2*, 2.5 mg/kg of body weight). Animals were killed and an autopsy was performed when they became moribund or when tumors grew to the German legal limit.

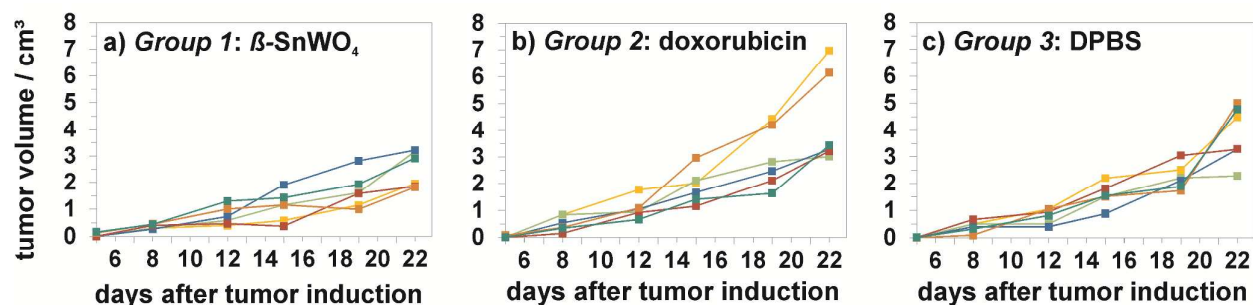
The tumor growth was monitored by measuring the tumor diameters with calipers twice a week. The tumor volume was calculated using the formula  $4/3 \cdot \pi \cdot a \cdot b \cdot c$  (ellipsoid). The treatment-related toxicity was determined by mouse weights weekly. Before the end of the study, 26 days after tumor induction, blood was collected *via* cardiocentesis. Tumor, inguinal and auxiliary lymph nodes were dissected, weighed and measured in size. The lung was macroscopically examined for the occurrence of metastases. Lung, tumor and lymph nodes were fixed overnight in 3.7% paraformaldehyd, embedded in paraffin and cut into sections for histological staining with hematoxylin and eosin. Animal procedures were approved by the regional government on animal experimentation in Germany: 35-9185.81/G-5/10.

Figure S4 and Figure S5 show the body weight and tumor growth of all animals as documented during the complete survey. The body weight for *group 1* ( $\beta$ -SnWO<sub>4</sub>-treated), *group 2* (doxorubicin-treated) and *group 3* (DPBS-treated) is rather constant during the complete survey. Slight increase of weight can be attributed to tumor growth.



**Figure S4. Body weight of tumor-bearing BALB/c-mice: a) *Group 1*–treated with  $\beta$ -SnWO<sub>4</sub> nanoparticles (23 mg/kg of body weight) and subsequently illuminated for 5 minutes with blue-light LED ( $\lambda_{max} = 465$  nm) at the site of the tumor; b) *Group 2*–treated with doxorubicin (2.5 mg/kg of body weight); c) *Group 3*–treated with DPBS (each value represents the mean of  $n = 6$  animals in the respective group).**

The tumor size of mice treated with physiological saline (DPBS, *group 3*) and doxorubicin (*group 2*) increased from day 1 to day 21 (Figure S5; *cf. main text: Figure 6*). In both cases some tumors grew to volumes up to 6 cm<sup>3</sup> (Figure S5; *cf. main text: Figure 6*). Moreover, only the control group and the doxorubicin-treated group showed cortically visible, broken-up tumors. As broken-up tumors continuously lose blood, they appear smaller than non-broken-up tumors. This explains the higher statistical spreading of the tumor volume of individual animals of the DPBS (*group 3*) and doxorubicin group (*group 2*). In contrast,  $\beta$ -SnWO<sub>4</sub>-treated mice (*group 1*) show a fundamentally reduced growth of the primary tumor (Figure S5; *cf. main text: Figure 6*). Moreover, all primary tumors remain at tumor volumes below 3 cm<sup>3</sup> and broken-up tumors were not observed for  $\beta$ -SnWO<sub>4</sub>-treated mice (*group 1*). Consequently, the statistical spreading between the different animals in this group is much narrower as compared to mice treated with physiological saline (DPBS, *group 3*) and doxorubicin (*group 2*) (Figure S5; *cf. main text: Figure 6*).



**Figure S5. Effect of  $\beta$ -SnWO<sub>4</sub> nanoparticles on the growth of the primary tumor. *Group 1*—treated with  $\beta$ -SnWO<sub>4</sub> nanoparticles (23 mg/kg of body weight) and subsequently illuminated for 5 minutes with blue-light LED ( $\lambda_{\max} = 465$  nm) at the site of the tumor; *Group 2*—treated with doxorubicin (2.5 mg/kg of body weight); *Group 3*—treated with DPBS (each value represents the mean of  $n = 6$  animals in the respective group). It is to be noted that broken-up tumors in the DPBS and doxorubicin group continuously lose blood and appear smaller than non-broken-up tumors, leading to certain spreading of the measured tumor volume.**

In addition to the  $\beta$ -SnWO<sub>4</sub>-treated mice (*group 1*) as well as the doxorubicin-treated mice (positive control, *group 2*) and DPBS-treated mice (negative control, *group 3*), the  $\beta$ -SnWO<sub>4</sub>-treated mice were, on the one hand, illuminated with a blue-light LED for 5 minutes at the site of the tumor (*group 1, with blue-light LED illumination*), and on the other hand, not illuminated with a blue-light LED (*group 1, without blue-light LED illumination*). While the data of mice treated with  $\beta$ -SnWO<sub>4</sub> nanoparticles with subsequent blue-light LED illumination were already discussed in the main text (*cf. main text: Figures 6-9*), data of mice treated with  $\beta$ -SnWO<sub>4</sub> nanoparticles but without blue-light LED illumination are shown in *Figures S6-S8*.

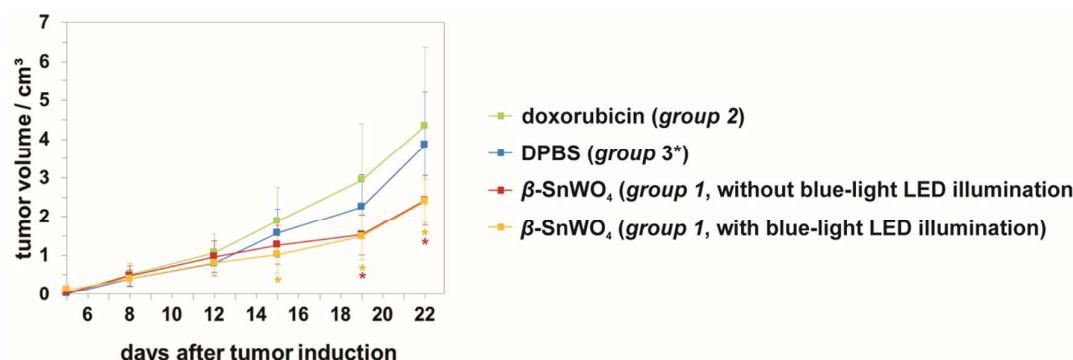


Figure S6. Effect of  $\beta$ -SnWO<sub>4</sub> nanoparticles on the growth of the primary tumor (*cf. main text: Figure 6*): *Group 1*—treated with  $\beta$ -SnWO<sub>4</sub> nanoparticles (23 mg/kg of body weight) with and without blue-light LED illumination; *Group 2*—treated with doxorubicin (2.5 mg/kg of body weight); *Group 3*—treated with DPBS (each value represents the mean of  $n = 6$  animals in the respective group; *SI: Figure S5* for detailed data on individual animals). Significance between the respective groups was determined according to student's  $t$ -test with  $p < 0.05$ . (\*) It is to be noted that broken-up tumors in the DPBS and doxorubicin group continuously lose blood and appear smaller than non-broken-up tumors, leading to certain spreading of the measured tumor volume.

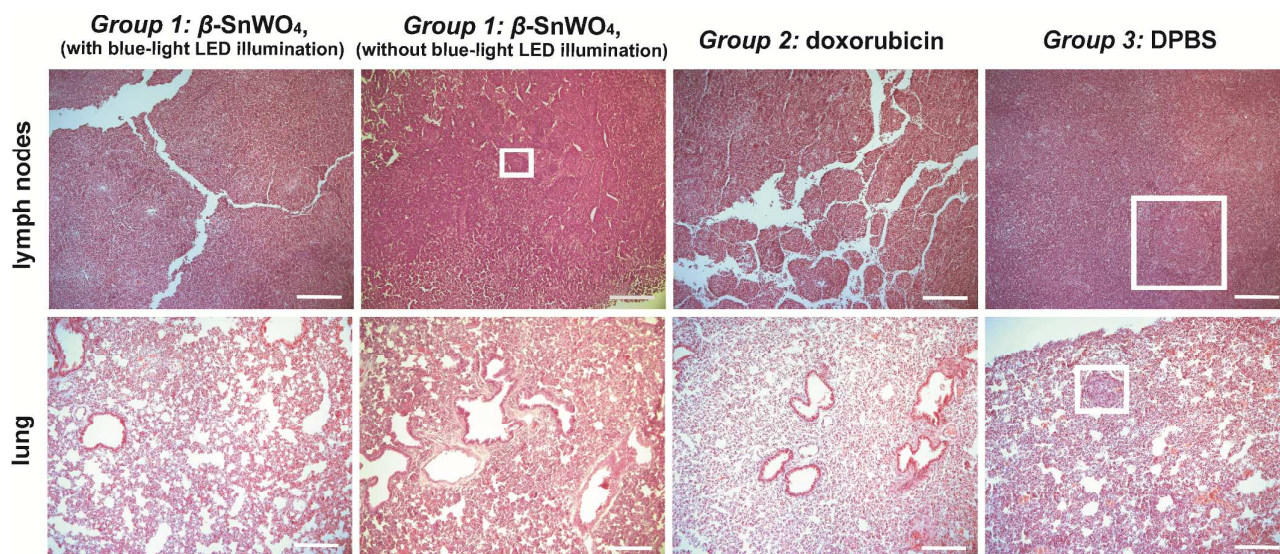
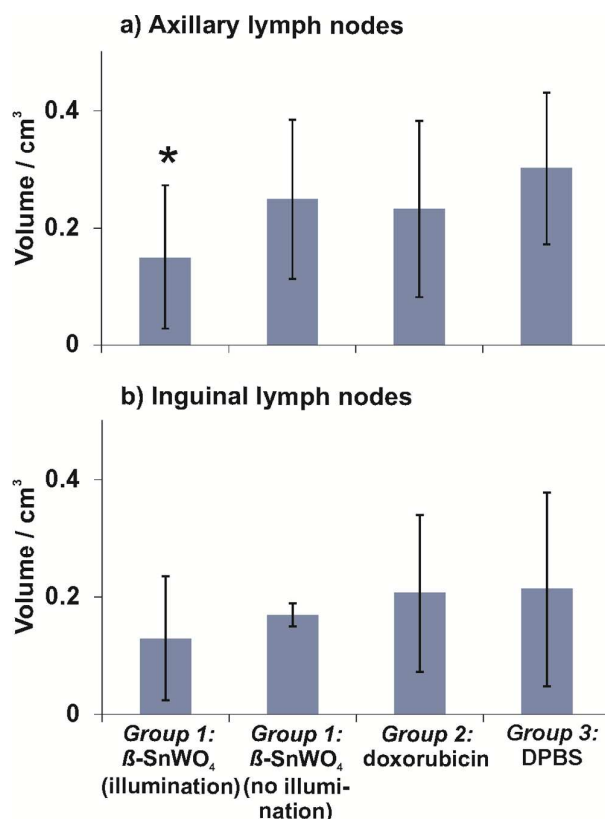


Figure S7. Effect of  $\beta$ -SnWO<sub>4</sub> nanoparticles on lymph-node metastasis (*cf. main text: Figure 8*): Qualitative histological analysis of lymph nodes and lungs with representative haematoxylin- and eosin-stained histological sections showing metastases for DPBS-treated mice only (see frame) (*group 1*,  $n = 6$ —treated with  $\beta$ -SnWO<sub>4</sub> nanoparticles with and without blue-light LED illumination; *group 2*,  $n = 6$ —treated with doxorubicin; *group 3*,  $n = 6$ —treated with DPBS as described in Figure 6; scale bar: 200  $\mu$ m).

To our surprise,  $\beta$ -SnWO<sub>4</sub>-treated mice show an almost similar significant decrease of the tumor volume independent of the blue-light LED illumination (*Figure S6*). However, this finding can be ascribed to the fact that living mice cannot be kept in the dark. Consequently, continuous daylight illumination (all day long) after injection of the  $\beta$ -SnWO<sub>4</sub> nanoparticles results in a comparable effect as short-timed (5 min), but direct and intense blue-light LED illumination (*Figure S6*). In fact, this is in accordance to previous *in vitro* studies<sup>1</sup> showing that  $\beta$ -SnWO<sub>4</sub> is also activated by daylight. Short-timed blue-light LED illumination is most effective for small sized tumors (<2 cm<sup>3</sup>, day 8 to day 18) that are completely transilluminated (*Figure S6*). Lymph-node metastasis (*Figure S7*) and lymph-node volume (*Figure S8*) as well indicate the influence of daylight illumination on mice that were treated with  $\beta$ -SnWO<sub>4</sub> nanoparticles but not illuminated *via* blue-light LED. The occurrence of lymph-node metastasis (*Figure S7*) as well as the significantly larger ipsilateral axillary and ipsilateral inguinal lymph nodes (*Figure S8*), on the other hand, clearly point to the effectiveness of the blue-light LED illumination.



**Figure S8.** Effect of  $\beta$ -SnWO<sub>4</sub> nanoparticles on lymph-node volume (*cf. main text: Figure 9*): a) Mean volume of ipsilateral axillary lymph nodes; b) Mean volume of ipsilateral inguinal lymph nodes (*Group 1, n = 6*—treated with  $\beta$ -SnWO<sub>4</sub> nanoparticles with and without blue-light LED illumination; *group 2, n = 6*—treated with doxorubicin; *group 3, n = 6*—treated with DPBS as described in *Figure 6*). The significance between the respective groups was determined according to student's *t*-test with  $p < 0.05$ .

#### 4. Blood parameters

The blood parameters as collected for all mice on the day of sacrifice are summarized in Table S1.

**Table S1. The blood parameters (MV ± SE, n = 6) were obtained from blood that was collected on the day of mice sacrifice. Significant aberrations as compared to values obtained in the control group are shown in red and tagged with (\*). Student's *t*-test served for calculation of significances (significance level  $p < 0.05$ ).**

	Unit	SnWO <sub>4</sub> , with LED illumination	SnWO <sub>4</sub> , no LED illumination	Doxorubicin	DPBS control	References <sup>8-12</sup>
<b>α-Amylase</b>	U/L	2187.5±303.8	2011.7±132.8	1898.7±132.4	1944.4±152.2	2035±355
<b>Lipase</b>	U/L	29.9±8.2	29.4±11.4	<b>53.0±24.3*</b>	25.3±3.9	901
<b>Fructosamines</b>	μmol/L	194.5±13.6	<b>289.7±10.9*</b>	171.3±31.0	194.1±16.0	
<b>Triglycerides</b>	mmol/L	1.6±0.2	1.5±0.1	1.6±0.5	1.2±0.4	1.15±0.40;1.02±0.18; 2.2
<b>Cholesterol</b>	mmol/L	2.0±0.2	1.9±0.1	2.1±0.4	1.8±0.5	2.31±0.41;2.6
<b>Bilirubin total</b>	μmol/L	2.6±0.6	2.4±1.8	2.3±0.5	3.3±3.1	5.99±2.22;7.2
<b>AP<sup>3</sup></b>	U/L	42.3±6.4	49.3±9.9	<b>23.2±5.9*</b>	38.8±8.1	139±43;129±28;84
<b>GLDH<sup>4</sup></b>	U/L	87.3±59.9	187.8±103.8	28.8±12.0	63.4±93.4	318±222;ca.13±3
<b>γ-GT<sup>5</sup></b>	U/L	1.3±1.8	1.1±0.7	0.7±0.5	1.5±2.3	
<b>ALT(GPT)<sup>6</sup></b>	U/L	147.2±92.6	112.4±34.0	144.3±85.5	85.2±36.6	24±10;49±5;34±4;61
<b>AST(GOT)<sup>7</sup></b>	U/L	242.1±94.3	449.1±267.2	226.5±76.5	186.8±89.5	47±13;150±17;140±13;75
<b>CK<sup>8</sup></b>	U/L	355.5±334.3	693.8±508.4	348.5±104.9	223.7±123.6	199±167.327
<b>Protein total</b>	g/L	54.3±3.7	55.7±0.6	<b>45.7±6.9*</b>	53.3±2.3	40.1±8.9;63
<b>Albumin</b>	g/L	33.0±3.8	33.2±1.0	29.3±4.3	30.6±3.4	33
<b>Globulines</b>	g/L	23.0±1.0	22.8±1.2	16.6±3.9	22.7±5.1	
<b>A/G-quotient</b>		1.3±0.0	1.3±0.0	<b>1.8±0.4*</b>	1.1±0.2	
<b>Urea</b>	mmoL/L	10.3±1.3	<b>7.1±0.6*</b>	11.0±0.7	12.5±3.4	7.92±3.41;9
<b>Creatinine</b>	μmol/L	19.6±5.0	16.8±1.3	16.8±6.5	16.9±3.4	19.45±16.80;10.2
<b>Phosphate-inorganic</b>	mmol/L	4.0±1.1	3.4±0.5	3.4±0.9	3.2±0.3	2.3
<b>Magnesium</b>	mmol/L	1.3±0.1	1.3±0.1	1.1±0.2	1.2±0.1	1.3
<b>Calcium</b>	mmol/L	2.5±0.2	2.6±0.2	<b>2.4±0.1*</b>	2.6±0.2	2.08±0.12;2.4
<b>Potassium</b>	mmol/L	8.9±1.4	12.7±1.8	8.7±1.1	31.8±51.6	4.40±0.96;6.6
<b>Sodium</b>	mmol/L	148.8±2.0	148.8±2.9	148.8±2.9	126.1±52.6	155.5±3.96;179.2
<b>Iron</b>	μmol/L	22.6±8.1	30.5±1.6	25.5±4.4	26.6±3.6	24.71
<b>Erythrocytes</b>	T/L	8.7±1.7	8.3±0.5	7.6±1.1	9.0±1.4	
<b>Hematocrit</b>	L/L	0.5±0.1	0.4±0.0	0.4±0.1	0.5±0.0	
<b>Hemoglobin</b>	g/L	130.8±21.9	125.3±5.5	<b>117.3±14.4*</b>	137.8±13.9	
<b>Leukocytes</b>	G/L	77.2±28.7	48.6±9.2	38.7±17.4	161.3±187.2	
<b>Segmented neutrophils</b>	%	<b>50.7±14.3*</b>	58.2±5.6	47.2±19.4	66.8±6.7	
<b>Lymphocytes</b>	%	30.3±10.8	24.5±6.8	28.2±19.7	26.8±6.4	
<b>Monocytes</b>	%	3.3±2.4	3.5±0.9	<b>1.7±1.1*</b>	3.5±1.3	
<b>Eosinophils</b>	%	<b>14.8±6.1*</b>	<b>9.7±1.8*</b>	<b>19.3±11.1*</b>	2.8±1.2	
<b>Basophiles</b>	%	<b>0.8±0.7*</b>	<b>1.5±1.0*</b>	<b>3.8±3.3*</b>	0.0±0.0	

<b>Unsegmented neutrophils</b>	%	0.0±0.0	0.0±0.0	0.0±0.0	0.0±0.0
<b>Hypochromasia</b>		neg	neg	neg	neg
<b>Anisocytosis</b>		neg	neg	neg	neg
<b>Thrombocytes</b>	G/L	225.0±56.7	247.7±36.1	215.7±53.9	293.8±136.3
<b>Segmented neutrophils</b>	G/L	36.9±14.2	28.4±6.5	17.6±10.1	116.4±146.6
<b>Lymphocytes</b>	G/L	25.6±17.4	11.6±2.8	13.4±0.175	33.6±26.4
<b>Monocytes</b>	G/L	2.43±1.7	3.2±1.2	0.5±0.5	6.6±9.8
<b>Eosinophils</b>	G/L	11.3±6.9	4.8±1.5	6.0±1.1	4.7±5.7
<b>Basophiles</b>	G/L	0.8±0.8	<b>0.7±0.5*</b>	<b>1.3±1.1*</b>	0.0±0.0
<b>Unsegmented neutrophils</b>	G/L	0.0±0.0	0.0±0.0	0.0±0.0	0.0±0.0

AP: alkaline phosphatase

GLDH: glutamate dehydrogenase

γ-GT: γ-glutamyl-transferase

ALT (GPT): alanine-amino-transferase (also: glutamic-pyruvate transaminase)

AST (GOT): aspartate aminotransferase (also: glutamic oxaloacetic transaminase)

CK: creatine kinase

## 5. Haematoxylin- and eosine- staining (progressive)

Paraffin-embedded organs were cut into 7 μm sections using a Leica RM 2155 microtome. Sections were transferred to slides and dried overnight at room temperature, and subsequently in an oven at 43 °C. Sections were stained and dehydrated according to the following protocol: The sections were incubated 2 · 5 minutes with xylene, 1 minutes with 100% ethanol, 2 · 1 minutes with 95% ethanol, 1 minutes with 70% ethanol, 3 minutes with distilled water, 7 minutes with haematoxylin (filtered), 3 minutes with distilled water, and 30 seconds with eosin. The sections were now rinsed with distilled water and again incubated with an increasing gradient of ethanol (2 · 1 minutes of 70%, 95%, 100% ethanol, respectively) and finally 2 · 1 minutes with xylene. Afterwards, sections were mounted, covered with a coverslip and dried overnight. Microscopy was performed with a Zeiss Axioskop.

## References

1. Ungelenk, J.; Feldmann, C. Synthesis of Faceted  $\beta$ -SnWO<sub>4</sub> Microcrystals with Enhanced Visible-Light Photocatalytic Properties. *Chem. Commun.* **2012**, *48*, 7838-7840.
2. Wang, C.; Ma, X.; Ye, S.; Cheng, L.; Yang, K.; Guo, L.; Li, C.; Li, Y.; Liu, Z. Protamine Functionalized Single-Walled Carbon Nanotubes for Stem Cell Labeling and *in vivo* Raman/Magnetic Resonance/Photoacoustic Triple-Modal Imaging. *Adv. Funct. Mater.* **2012**, *22*, 2363-2375.
3. Liscovitch, M.; Lavie, Y. Cancer Multidrug Resistance: A Review of Recent Drug Discovery Research. *Drugs* **2002**, *5*, 349-355.

4. Nichols, J. W.; Bae, Y. H. Odyssey of a Cancer Nanoparticle: From Injection Site to Site of Action. *Nano Today* **2012**, *7*, 606-618.
5. Gabizon, A.; Tzemach, D.; Mak, L.; Bronstein, M.; Horowitz, A. T. Dose Dependency of Pharmacokinetics and Therapeutic Efficacy of PEGylated Liposomal Doxorubicin (DOXIL) in Murine Models. *J. Drug Target.* **2002**, *10*, 539-548.
6. Kim, E. J.; Lim, K. M.; Kim, K. Y.; Bae, O. N.; Noh, J. Y.; Chung, S. M.; Shin, S.; Yun, Y. P.; Chung, J. H. Doxorubicin-Induced Platelet Cytotoxicity: A New Contributory Factor for Doxorubicin-Mediated Thrombocytopenia. *J. Thromb. Haemost.* **2009**, *7*, 1172-1183.
7. Fleig, S. in: Medizinischen Fakultät, Charité - Universitätsmedizin Berlin, Berlin 2011.
8. Kim, M. J.; Kim, H. K. Effect of Garlic on High Fat Induced Obesity. *Acta Biol. Hung.* **2011**, *62*, 244-254.
9. Le Minh, K.; Klemm, K.; Abshagen, K.; Eipel, C.; Menger, M. D.; Vollmar, B. P. Prophylaktische wie auch therapeutische Gabe von Darbeпоetin alpha wirkt anti-inflammatorisch und anti-apoptotisch im Modell des akuten septischen Leberschadens der Maus. *Chirurg. For.* **2007**, *36*, 205-207.
10. Mazzaccara, C.; Labruna, G.; Cito, G.; Scarfo, M.; De Felice, M.; Pastore, L.; Sacchetti, L. Age-Related Reference Intervals of the Main Biochemical and Hematological Parameters in C57BL/6J, 129SV/EV and C3H/HeJ Mouse Strains. *PloS one* **2008**, *3*, e3772.
11. Schledzewski, K.; Geraud, C.; Arnold, B.; Wang, S.; Grone, H. J.; Kempf, T.; Wollert, K. C.; Straub, B. K.; Schirmacher, P.; Demory, A.; *et al.* Deficiency of Liver Sinusoidal Scavenger Receptors Stabilin-1 and -2 in Mice Causes Glomerulofibrotic Nephropathy *via* Impaired Hepatic Clearance of Noxious Blood Factors. *J. Clin. Invest.* **2011**, *121*, 703-714.
12. Zur, B. in: Institut für Klinische Chemie und Laboratoriumsdiagnostik, Heinrich-Heine-Universität Düsseldorf, Düsseldorf 2005.